Atmospheric Environment 45 (2011) 6057–6069

Contents lists available at ScienceDirect

Atmospheric Environment

journal homepage: www.elsevier.com/locate/atmosenv

Validation of modeled carbon-dioxide emissions from an urban neighborhood with direct eddy-covariance measurements

A. Christen [a,*], N.C. Coops [b], B.R. Crawford [a], R. Kellett [c], K.N. Liss [a,d], I. Olchovski [c], T.R. Tooke [b], M. van der Laan [a,c], J.A. Voogt [e]

[a] Department of Geography, University of British Columbia, 1984 West Mall, Vancouver, BC V6T 1Z2, Canada
[b] Faculty of Forestry, University of British Columbia, 2424 Main Mall, Vancouver, BC V6T 1Z4, Canada
[c] School of Architecture and Landscape Architecture, University of British Columbia, 2357 Main Mall, Vancouver, BC V6T 1Z4, Canada
[d] Department of Natural Resource Sciences, McGill University, 21 111 Lakeshore Road, Montréal, QC H9X 3V9, Canada
[e] Department of Geography, University of Western Ontario, 1151 Richmond Street, London, ON N6A 5C2, Canada

ARTICLE INFO

Article history:
Received 8 November 2010
Received in revised form
18 July 2011
Accepted 22 July 2011

Keywords:
GHG emission modeling
Building energy modeling
Carbon-dioxide
Flux measurements
Eddy-covariance
LiDAR
Model validation

ABSTRACT

Modeled carbon-dioxide (CO_2) emissions from an urban area are validated against direct eddy-covariance flux measurements. Detailed maps of modeled local carbon-dioxide emissions for a 4 km^2 residential neighborhood in Vancouver, BC, Canada are produced. Inputs to the emission model include urban object classifications (buildings, trees, land-cover) automatically derived from Light Detection and Ranging (LiDAR) and optical remote sensing in combination with census, assessment, traffic and measured radiation and climate data. Different sub-models for buildings, transportation, human respiration, soils and vegetation were aggregated. Annual and monthly CO_2 emissions were modeled on a spatial grid of 50 m for the entire study area. The study area overlaps with the source area of a micrometeorological flux tower for which continuous CO_2 flux data (net exchange) were available for a two-year period. The measured annual total was 6.71 kg C m^{-2} $yr^{-1}$with significant seasonal differences (16.0 g C m^{-2} day^{-1} in Aug vs. 22.1 g C m^{-2} day^{-1} in Dec correlated with the demand for space heating) and weekday-weekend differences (25% lower emissions on weekends attributed to traffic volume differences). Model results were weighted using the long-term turbulent source areas of the tower. Annual total modeled (7.42 kg C m^{-2} yr^{-1}) and measured emissions agreed within 11%, but show more substantial differences in wind sectors dominated by traffic emissions. Over the year, agreement was better in summer (5% overestimation by model) vs. winter (15% overestimation), which is partially attributed to climate differences unaccounted for in the building energy models. The study shows that direct CO_2 flux measurements based on the EC approach - if sites are carefully chosen - are a promising method to validate fine-scale emission inventories/models at the block or neighborhood scale and can inform further model improvements.

1. Introduction

Roughly 30–40% of all direct anthropogenic greenhouse gas (GHG) emissions originate directly from within urbanized areas (Satterthwaite, 2008). Combustion of fossil fuels and the resulting emission of carbon-dioxide (CO_2) in the transportation, industry and residential sectors is the most dominant process responsible for direct anthropogenic GHG emissions in urban environments. A detailed attribution of CO_2 emissions to specific urban activities is challenging due to the spatial separation of energy, resource and goods production and consumption. Nevertheless, significant inter- and intra-urban differences in per-capita CO_2 emissions are evident when comparing inhabitant activities and associated consumption patterns in various studies (e.g. Kennedy et al., 2009; Soegaard and Moller-Jensen, 2003). As much as 50% of CO_2 emissions in cities are attributable to urban form choices - notably density, land-use mix, building types, transportation networks, and vegetation. Salat (2007) and Baker and Steemers (2000), for example, argue that urban form variation can influence urban building energy demand by factors up to a factor of 2.5 and urban energy systems performance can vary up to a factor of 2. Newman and Kenworthy (1989) and Kennedy at al (2009) identify urban density and automobile usage as key controls of per-capita fuel consumption in various global cities. VandeWeghe and Kennedy (2008) show for Toronto

* Corresponding author.
E-mail address: andreas.christen@ubc.ca (A. Christen).

1352-2310/$ – see front matter © 2011 Elsevier Ltd. All rights reserved.
doi:10.1016/j.atmosenv.2011.07.040

a similar relation at the neighborhood scale– generally increasing transportation-related per-capita CO_2 emissions with decreasing urban density of census districts.

1.1. Modeling GHG emissions from urban areas

Planning policy and regulation are powerful instruments to promote urban form and transportation strategies that reduce energy consumption and GHG emissions. Appropriate models are required to evaluate the impact of, and opportunity for, urban planning and design scenarios for all relevant components that emit or uptake CO_2 in urban ecosystems – including buildings, transportation, food, goods, waste, soils, and vegetation. It can be expected that integrative decision support, where net effects of various emission components are considered and compared, will become an increasingly relevant part of urban planning processes in the future (Grazi and van den Bergh, 2008).

A particular challenge is to formulate the appropriate models and CO_2 emission estimates at fine spatial scales (100 m–5 km). These scales are important for urban design decisions which are often required at neighborhood, block, or building scale, however modeling of the geographical distribution of emissions is typically done using consumption statistics that are available at much coarser spatial scales (national, provincial/state, municipal) and scaled down using proxy data such as land-cover, population density, or nightlights (e.g. Raupach et al., 2009; Parshall et al., 2010).

1.2. Direct flux measurements of GHGs in urban areas

Direct flux measurements of GHGs using the eddy-covariance (EC) approach could provide a valuable method to validate fine-scale urban emission inventories and model estimates at the scale where planning decisions are made (100 m–10 km, e.g. building codes, land-use, public transportation). EC is currently used at several hundred research sites worldwide to continuously monitor CO_2 fluxes between various natural and managed ecosystems and the atmosphere, including farm land, grasslands, tundra, and forests (e.g. Baldocchi, 2003). Despite methodological challenges due to the complex source configuration and variation, and the extreme variability of form in urban areas (Grimmond et al., 2002), more than thirty studies have reported successful and meaningful CO_2 flux measurements based on the EC approach over selected urban neighborhoods (Val and Roth, 2010). Many of those studies report short-term measurements over a few weeks, and but only few studies so far have been published that report year-long flux measurements. The objective of this contribution is to evaluate if EC measurements in combination with source-area models can provide spatiotemporal information to validate fine-scale emission data at scales where utility or consumption data is not available or is challenging to access due to privacy and logistical reasons.

However, there are several limitations to EC measurements. EC of greenhouse gases in cities is currently limited to CO_2 - with the notable exception of a short-term study on urban nitrous oxide (N_2O) emissions in the city of Edinburgh (Famulari et al., 2010). Values reported are hence just emissions of CO_2 and not carbon-dioxide equivalents (CO_2e, i.e. including N_2O and CH_4 emissions). Also, the EC method cannot be used to validate solely building energy models or transportation models as it quantifies the total CO_2 emitted from an urban area without identifying the specific sources and sinks. Flux measurements also include carbon released and absorbed by ecological processes including human and microbial respiration, and photosynthesis. Finally, the EC approach only quantifies locally emitted sources, and cannot account for external emissions due to local activities – such as power plant emissions outside the source area of the EC system as a consequence of power consumption within the area.

The objective of this paper is to present, evaluate and discuss an approach for validating spatially modeled local emissions at a fine-scale with direct EC measurements using a case study area in Vancouver, British Columbia, Canada.

2. Methods

2.1. Case study area

The area modeled is a primarily residential area of 1900 m by 1900 m in south central Vancouver – centered on the EC tower 'Vancouver-Sunset' (494290, 5452601, UTM-10, Fig. 1). Of the total plan area of the study area, 29% is building footprints, 11% is tree covered (17.1 trees ha^{-1}), 24% is ground vegetation (predominantly lawns) and 35% is non-vegetated ground surfaces (streets, sidewalks, driveways).

The total population in the study area is 23,166 (64.2 inhabitants ha^{-1}). Within the study area are 4558 buildings of which 4155 are residential single-family dwellings (SFD). Due to high demand for additional rental space in Vancouver, approximately 55% of the SFD have secondary suites (additional rental units within existing single-family homes). As a consequence, with an average of 4.6 inhabitants per SFD, the occupancy is substantially above the Canadian national average of 2.6 per dwelling. The high occupancy will likely decrease per-capita emissions and increase per-area emissions when compared to other single-family developments. 37% of residential dwellings in the study area were built before 1965, 38% between 1965 and 1990, and 25% post 1990. The average conditioned floor area of the residential dwellings is 202.7 m^2.

The area has an orthogonal street grid, with commercial and higher density residential nodes and corridors concentrated along a few arterial streets. In particular Knight Street, which transects the study area from North to South, is a major truck and commuter route to and from Vancouver (58,000 vehicles day^{-1}). Three public parks (Memorial South Park, Gordon Park, Tecumseh Park), cover 7% of study area and contain 20% of the total ground and tree leaf area.

The study period encompasses two years from May 1, 2008 to April 30, 2010. The climate of the study area is considered oceanic (Csb, Köppen-Geiger), with average air temperature (canopy layer) of 10.8 °C with dry summers (284 mm from Apr to Sep) and a precipitation maximum in winter (832 mm from Oct to Mar, Table 1). The regional temperatures during the study period (measured at the Vancouver International Airport, WMO ID 71892) were 0.2 K warmer than the 30-year climatological average (1971–2000). Precipitation over the study period (1117 mm yr^{-1}) was 7% less than the 30-year average (1199 mm yr^{-1}).

2.2. Emission modeling approach

The model is a combination of top-down inventory and bottom-up modeling of individual objects (buildings, vegetation, traffic counts). Carbon is tracked by quantifying inputs and outputs into the modeled urban neighborhood, as well as storage changes within the neighborhood. Inputs and outputs happen at different boundaries (lateral, vertical) and in different chemical forms (e.g. carbohydrates, CO_2). The complete carbon emission model and its application is described in Christen et al. (2010).

In this contribution we are solely interested in the vertical exchange, i.e. emissions and uptake of CO_2– as vertical fluxes can be measured using the EC approach on towers. In an urban ecosystem, vertical fluxes are expected to be dominantly CO_2 emissions from fossil fuel combustion, but also include respiratory

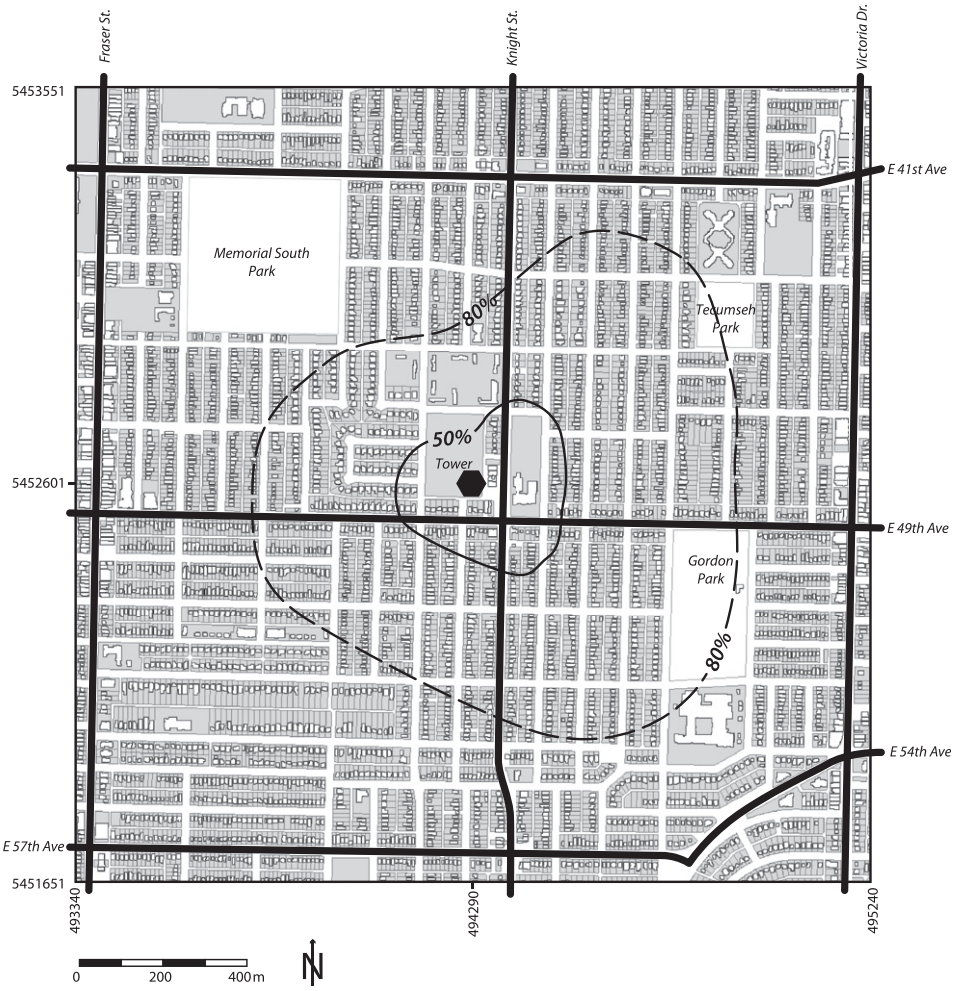

Fig. 1. Map of the study area with arterial roads (thick black lines), tower location (hexagon in centre). Overlaid are the integrated long-term (May 2008–Apr, 2010) turbulent source area encircling 50% and 80% of the area where tower fluxes originate.

release and CO_2 uptake by urban vegetation. The spatial modeling of vertical fluxes is separated into four components – (i) buildings, (ii) transportation, (iii) human respiration and (iv) vegetation/soils - that are illustrated along with their corresponding model inputs in Fig. 2.

Gridded Light Detection and Ranging (LiDAR) data at 1 m resolution (Goodwin et al., 2009) and satellite data (Quickbird Multispectral Sensor at 2.4 m spatial resolution, see Tooke et al., 2009) are used as detailed inputs for deriving urban form and cover parameters relevant for emission modeling. Information on

Table 1
Average conditions and EC system coverage during the measurement period May 2008 to April 2010. Months are averages of two years. Air temperature was measured continuously at 2 m height in the urban canopy layer, soil temperatures/soil volumetric water content are an average of thermistors/TDRs (CS616, Campbell Scientific) installed in four representative lawns in the study area at 5 cm depth. Indoor temperatures are the average of air temperatures continuously monitored in the living space of four residential SFD within the study area. Heating degree days are calculated with a threshold temperature of 18 °C. Precipitation was measured at Vancouver international airport, short-wave irradiance (CNR-1, Kipp & Zonen) was measured on top of the EC tower at a height of 26 m above ground.

	Average air temperatures (°C)	Average soil temperatures (°C)	Average indoor temperatures (°C)	Heating degree days (°C day)	Average short-wave irradiance (MJ m^{-2} day^{-1})	Precipitation (mm $month^{-1}$)	Average soil volumetric water content (m^3 m^{-3})	EC data Coverage (%)
Jan	4.5	4.2	18.7	419	3.1	156	0.38	56.5%
Feb	5.8	5.6	18.4	342	6.5	80	0.36	73.8%
Mar	6.2	7.1	18.4	366	10.2	106	0.37	72.7%
Apr	9.8	11.3	19.2	246	16.1	83	0.34	74.0%
May	13.5	15.4	21.0	140	20.1	58	0.27	76.7%
Jun	16.4	18.3	22.3	48	21.2	27	0.18	68.8%
Jul	19.6	20.8	24.0	0	23.0	18	0.16	87.8%
Aug	18.4	20.0	23.3	0	17.9	51	0.21	73.4%
Sep	15.7	16.4	21.6	69	13.9	48	0.22	81.2%
Oct	10.1	11.3	19.8	245	7.4	123	0.30	71.0%
Nov	7.5	8.1	19.7	315	3.0	230	0.36	57.9%
Dec	1.6	3.3	19.1	508	2.8	137	0.36	46.7%
Full 2-year period	10.8 °C	11.8 °C	20.4 °C	2697 °C day	4.31 GJ m^{-2} yr^{-1}	1,117 mm yr^{-1}	0.30 m^3 m^{-3}	70.0%

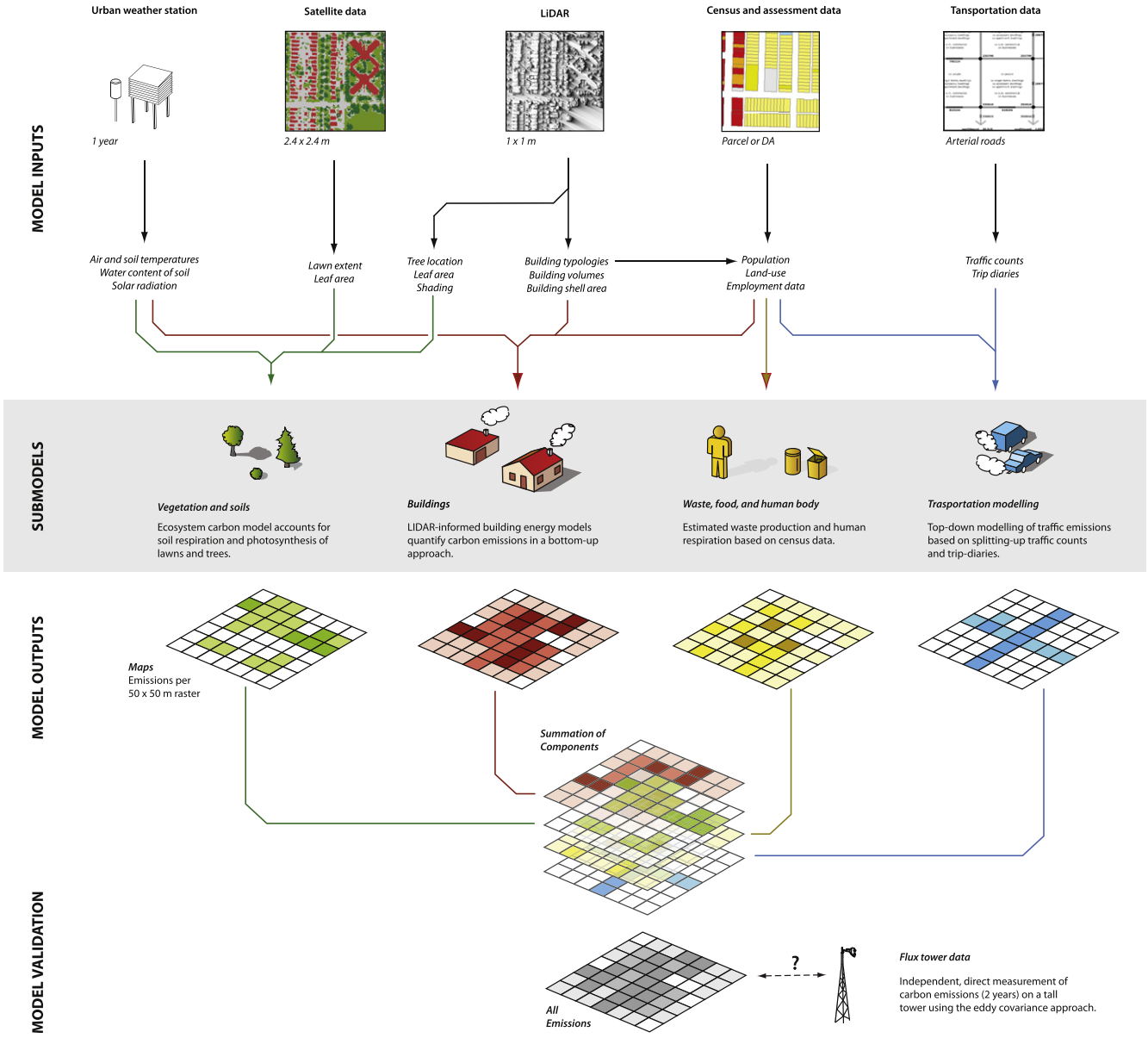

Fig. 2. Diagrammatic representation of the emission modeling approach. At the centre (grey band) are the four metabolism components or sub-models — vegetation and soils, buildings, human metabolism and transportation. At the top, are the data sources from which sub-model inputs are derived and aggregated. Below are model outputs that are modeled carbon emissions estimates expressed in quantitative (how much) and spatial (where) terms. At the bottom is the model validation step against EC measurements.

surface cover fractions, building dimensions, building form and volume as well as vegetation characteristics (height, density) were extracted and spatially mapped. Based on this information, which is available for the entire study area, maps of total annual CO_2 emissions (or uptake) are modeled at 50 m resolution. Maps from all four sub-models (building, transportation, human respiration and vegetation) are then summed to create a map of integral (net) emissions at 50 m resolution (Fig. 2, bottom). Those net-emissions are then compared to direct tower measurements.

2.2.1. Emissions from buildings

This component includes stationary combustion sources transforming fossil fuel carbon (natural gas, heating oil) into CO_2 for space heating or cooling, hot water, lighting, space cooling, and auxiliary equipment loads. A bottom-up building-typology approach was used to describe the study neighborhood through a series of building prototypes that are characteristic of the existing building stock. Through fieldwork and informed by LiDAR extracted urban form statistics, two overarching building categories emerged for the study area (residential and 'other,' non-residential) along with thirteen sub-types. Of the 4558 buildings sampled in the study area, 95% were residential. Residential buildings were further divided into four additional categories: apartments, row houses, duplexes and single-family detached (SFD). SFD then were further divided in three sub-types based on year of construction and the presence of secondary suites.

To estimate CO_2 emissions, two separate building energy models (BEM), one dedicated to ground oriented residential sub-types (HOT2000) and one for 'other' building types (OEE Screening tool) were run on a monthly time step. HOT2000 outputs monthly total emissions based on a monthly climatology. HOT2000 is well suited for the residential building types found in the study area. It

has been validated extensively against hourly simulation programs such as DOE2.1 and Blast3.0 (Haltrecht and Fraser, 1997). The model however, lacks the ability to calculate time-steps smaller than one month and therefore was the limiting temporal factor when comparing modeled and measured data. The Office of Energy Efficiency (OEE) Screening tool was developed to evaluate commercial and institutional building energy use relative to the Model National Energy Code for Buildings (MNECB) and provides building energy consumption estimates by fuel type and end use based on a limited number of inputs including building size, type, insulation, energy demand and system efficiencies (Natural Resources Canada, 2010).

In order to provide HOT2000 with locally relevant inputs for the study area attributes were extracted from LiDAR data and house audits. Actual morphological parameters and heated floor area were extracted from LiDAR data individually for each building. Statistical data and house audits (12 in total provided by Natural Resources Canada) informed typical insulation, air-tightness, heating system and efficiency. In the study area, a large part of residential energy use is dedicated to space heating. The majority (94%) of single-family homes and duplexes in the study area are heated by natural gas (emission factor of 13.9 kg C GJ^{-1}). The secondary heating source for residential development is electricity - which becomes more prevalent in attached and stacked dwellings. Electricity also provides power for building lighting, auxiliary equipment, space cooling and hot water. However, as CO_2 emissions associated with electricity consumption are not occurring within the neighborhood, they will not be included in the comparison with tower EC measurements. Further, the external emissions due to power generation are substantially less than natural gas due to the large proportion of hydroelectric power generation (1.67 kg C GJ^{-1}; Province of British Columbia, 2008). Fireplaces are present in 85% of all SFD, but are not a primary heating source.

2.2.2. Emissions from transportation

The transportation sub-model estimates the fossil fuel combustion that occurs locally in the study area by vehicle trips to, from and through the study area. Within the study area were 13 directional traffic count sites with one or more sets of recent 24-h weekday traffic counts and nine intersection traffic movement counts with a few hours of peak travel data. Data gathered at these points were used to construct a weekday traffic profile for the entire study area. In this profile all vehicle trips were assumed to enter or exit the study area along one of the arterial roads (see Fig. 1, dark lines) for which counts were available. Trip diaries by the British Columbia Ministry of Transportation and Greater Vancouver Transportation Authority (2004) were used to estimate the local trip share as 24% and through trips at 76% of total trips. At a central intersection at the northern part of the study area a vehicle class traffic count was available and is used to estimate vehicle types on arterials. Four vehicle types were considered (light, transit, medium freight and heavy freight vehicles) and standard fuel efficiencies were used (Natural Resources Canada, 2009) to estimate the CO_2 emitted for each trip and vehicle type within the study area. The monthly traffic profile was constructed using five-year average traffic counts from four automatic systems on arterial highways and roads located outside the study area (BC Ministry of Transportation and Infrastructure). At those sites, traffic showed a distinct annual course with highest volume in summer (June: 104% of annual average) and lowest in January (94% of annual average). Those percentages were used to scale monthly emissions based on the annual total.

2.2.3. Emissions due to human respiration

CO_2 emitted by human respiration, is measured on the tower, and hence it was included in the modeling approach as an emission into the atmosphere. The injection of CO_2 by human respiration into the atmosphere was calculated using a night-time population distribution (Statistics Canada, 2007) that was spatially distributed using residential floor area (calculated from LiDAR volume and land-use data) as proxy. The night-time population distribution was simply multiplied by a typical annual respiration of a human body of 76.3 kg C yr^{-1} cap^{-1} (Moriwaki and Kanda, 2004).

2.2.4. Emissions and uptake by vegetation and soils

This component can act as sink or source through photosynthesis and respiration. The ability of urban vegetation to uptake fossil fuel carbon in urban biomass and soils make this component relevant. The fluxes in this component were calculated separately for (i) the process of respiration and (ii) photosynthesis and separately for (a) tall vegetation (bushes, trees) and (b) ground vegetation/soils (predominantly lawns). Respiration from soils and lawns was modeled based on empirical relations derived from 280 manual chamber measurements (40 locations) taken between 7 and 18h local time in summer and winter 2008/09. The chamber measurements encompass the range of soil temperatures and soil volumetric water content in the study period. Respiration was modeled as a function of soil temperature and volumetric water content following Liss et al. (2009). The lawn and soil fraction used to upscale to the neighborhood scale was extracted from high-resolution remote sensing data following Tooke et al. (2009) taking into account respiration from soil below trees. The respiration model was driven in 5 min steps by measured soil temperatures and soil volumetric water content data (4 locations each) for the entire year of 2009.

Respiration from above ground biomass was modeled based on measurements from a portable photosynthesis measurement system (Li-6400, Licor Inc., Lincoln, Nebraska, USA) measuring dark respiration of leaves/needles of a total of 12 representative urban trees and shrubs in the study area (Sugar Maple, Purple Leaf Flowering Plum, Dwarf and Rosebay Rhododendron, Cherrylaurel, American Chestnut, Oregon Ash, European Beech, American Elder and Silver Maple). Above ground respiration was scaled up from leaf to neighborhood scale using a LiDAR-derived leaf area index (LAI) and year-round climate data at 5 min steps. The average LAI of trees for the entire study ground area was 0.39 m^2 m^{-2} and of lawns 1.44 m^2 m^{-2}. LAI of trees was estimated using gridded LiDAR data at 1 m resolution in combination with allometric relationships (Nowak, 1996). LAI of lawns was estimated based on destructive sampling (Liss et al., 2010). Of all trees and bushes in the study area, 23% were evergreen, and 77% were deciduous.

CO_2 uptake by photosynthesis of lawns was modeled based on photosynthetically active radiation (PAR) irradiance and light-response curves (Ögren and Evans, 1993), with actual parameters fitted through 255 clear-chamber measurements at 40 locations. Actual photosynthesis was taking into account shading and reduction of photosynthetic activity due to water stress (empirical relation vs. measured soil volumetric water content). For 5-min steps, PAR irradiance was estimated on a 1 x 1 raster for all lawn surfaces in the neighborhood based on the gridded LIDAR dataset and using solar geometry and measured short-wave irradiance above the canopy. Photosynthesis by trees was modeled based on measured light-response curves from 12 representative trees in the neighborhood that were combined with a multi-layer radiation transmission model at 1 m^3 resolution using LIDAR estimated LAI. Photosynthesis was scaled up from leaf to neighborhood scale using year-round climate data at 5-min resolution.

More important than direct carbon sequestration, however, are indirect effects of urban vegetation (shading, sheltering) that can reduce/increase energy demand for space heating and cooling of buildings (e.g. McPherson, 1994; Akbari et al., 2001; Simpson,

2002). Those effects have been included in the building energy subcomponent (Section 2.2.1) by choosing appropriate shading and sheltering inputs.

2.3. Direct carbon flux measurements

2.3.1. Site, instrumentation and processing

The EC system used in this study to measure carbon fluxes is located in the centre of the chosen study area on a triangular open lattice tower, 28.8 m above the local ground surface. The source area of this tower platform was identified in previous research as a flat and relatively homogeneously developed urban area and was extensively used in many micrometeorological studies on the urban energy and water balance (e.g. Kalanda et al., 1980; Cleugh and Oke, 1986; Roth et al., 1989). For CO_2, however, model results (Section 3.1) and CO_2 EC measurements from a previous study at the same location (Walsh, 2005) suggest that the homogeneity hypothesis does not hold and a more detailed source area attribution is required to aggregate fluxes.

Data used in this study was continuously sampled from May 2008 to April 2010. The instrumentation used consists of a sonic anemometer (CSAT 3-d sonic anemometer, Campbell Scientific, Logan, UT, USA) and an open-path infrared-gas analyzer (Li-7500, Licor Inc., Lincoln, NE, USA). Three dimensional wind velocities and CO_2 concentrations are sampled at 20 Hz and are stored on a data logger (CR3000, Campbell Scientific, Logan, UT, USA) for further post-processing. Vertical fluxes of CO_2 (F_c) were calculated as the covariance of vertical wind component and the instantaneous deviation from the mean CO_2concentration as described in Velasco and Roth (2010). Before calculation, the coordinate system of the wind velocity components is rotated two times for each block separately and the 30-min average is corrected to account for changes in air density (Webb et al., 1980) and spatial separation between gas-analyzer and anemometer (Moore, 1986). Fluxes undergo several additional quality control checks (sensor diagnostics, spike detection, statistics within limits), with all details given in Crawford et al. (2010). Using this procedure, 30-min values of F_c were calculated for all 30 min blocks in the full 2-year cycle. Data coverage for the 2-year period is 70.0% (26.6% of data loss is due to weather, 3.4% due to system failure, Table 1).

2.3.2. Aggregation of monthly and annual fluxes

To retrieve monthly and annual flux densities (net exchange), 30-min fluxes of F_c in g C m^{-2} s^{-1} were averaged and spatially sorted to account for different emission characteristics across the source area. Each valid 30-min block average is sorted by (i) month of the year m, (ii) hour of the day h, and (iii) wind direction (vector wind average) into one of four wind sectors ω, NE (0–90°), SE (90°–180°), SW (180°–270°), and NW (270°–360°). For each hour of the day h, each month, and each wind sector ω an ensemble average flux is calculated:

$$\langle F_c\rangle_{h,m,\omega} = \frac{1}{N\bar{I}}\sum_{t=1}^{N} I(t)\,F_c(t) \tag{1}$$

where I is an indicator function that is equal to one if for the time step of interest, wind was from a given sector ω, given month m and within a selected hour h, and zero otherwise. $\bar{I}$ is the average of I over the entire study period (fractional occurrence). This averaging approach assumes that there are enough cases in each conditional average (each wind sector, each hour, each month). Running the approach on shorter time periods (e.g. weeks, days) would result in too many conditions without occurrence and/or low statistical representation. The few cases without any occurrence of the wind direction ($\bar{I} = 0$) were linearly interpolated along the hourly time axis for up to 3 h using nearest ensemble averages earlier or later in the diurnal course (cyclic). The average diurnal course of each month was then integrated over a full day to retrieve a daily CO_2 flux in g C m^{-2} day^{-1} for each wind sector and each month:

$$\langle F_c\rangle_{m,\omega} = 3600\sum_{h=1}^{24}\langle F_c\rangle_{h,m,\omega} \tag{2}$$

The factor 3600 converts g C m^{-2} s^{-1} to g C m^{-2} h^{-1}. The average of the 'entire' neighborhood in a given month was calculated by averaging all four wind sectors:

$$\langle F_c\rangle_{m} = \frac{1}{4}\sum_{\omega=1}^{4}\langle F_c\rangle_{\omega,m} \tag{3}$$

For the annual total flux density in a given wind sector, monthly averages in g C m^{-2} day^{-1} from the given sector were integrated and weighted by the number of calendar days $D(m)$ in each month to give an annual total in g C m^{-2} yr^{-1}:

$$\langle F_c\rangle_{\omega} = \sum_{m=1}^{12} D(m)\langle F_c\rangle_{m,\omega} \tag{4}$$

The above procedure was separately applied for weekdays (Mon–Fri) and weekends (Sat–Sun) as transportation emissions were expected to vary. Flux densities integrated over the entire neighborhood (all wind sectors) and year were calculated similarly to Eq. (3) as the equally weighted, yearly total flux from each of the four wind sectors.

2.3.3. Turbulent source areas

A 2-dimensional gradient diffusion and crosswind dispersion model (Kormann and Meixner, 2001) was run for all 30 min periods between May 1, 2008 and April 30, 2010 at a 2 m grid resolution over a domain of 2000 by 2000 m, upscaled to 50 m resolution to match the emission maps and cropped to the 1900 by 1900 m domain of the study area. The long-term integrated source area was calculated as the average of all individual (changing) 30-min source areas during that period (according to Chen et al., 2009).

Flux footprints (or vertical flux per unit point source) $\phi\ (x,y)$ were calculated in a gridded format at 2 m resolution for each 30 min step and then scaled up to 50 m. Each individual grid cell was summed using the same process by which fluxes were aggregated i.e. for each hour h of the day, each month of the year m and each of the four wind sector ω. This was achieved by replacing F_c in Eq. (1)–(4) with values from the 50m grid of the individual $\phi\ (x,y)$ fields resulting in ensemble average flux footprint $\langle\phi\rangle\ (x,y)$ for different months, the entire year and the various wind sectors.

In a next step, modeled emissions on the 50 m grid $M_c\,(x,y)$ were weighted by the ensemble flux footprint by multiplying total emissions from each grid cell with the ensemble average flux footprint grid $\langle\phi\rangle\ (x,y)$ and integrating over the entire study area (1900m):

$$[M_c]_{in} = \int_{x=0m}^{1900m}\int_{y=0m}^{1900m}\langle\phi(x,y)\rangle M_c(x,y)\,dx\;dy \tag{5}$$

A small fraction of the flux footprint is predicted to be outside the 1900 by 1900 m study area and the integrated $\langle\phi\rangle\ (x,y)$ within the study area is lower than unity. For the entire year, the fraction of the flux footprint outside the study $[\phi]_{out}$ area was 12%:

$$[\phi]_{out} = 1 - \left(\int_{x=0m}^{1900m} \int_{y=0m}^{1900m} \langle \phi(x,y) \rangle \, dx \; dy \right) \quad (6)$$

This fraction was set to the average modeled emissions within the entire study area $[M_c]_{out}$. This approach assumes that the urban form continues in a similar pattern outside the study area. The total modeled emission for a given ensemble situation is then:

$$[M_c]_{tot} = [M_c]_{in} + [\phi]_{out}[M_c]_{out} \quad (7)$$

3. Results and discussion

3.1. Modeled emissions

3.1.1. Buildings

According to the bottom-up estimate of the BEM, buildings emit a total of 2.47 kg C m^{-2} yr^{-1} within the study area. 2.15 kg C m^{-2} yr^{-1} are modeled from residential buildings and 0.32 kg C m^{-2} yr^{-1} from commercial and institutional ones. CO_2 emissions varied for different building typologies, and were, for example 11.1 kg C $yr^{-1}m^{-2}$ floor area in older (pre-1965) SFD, 9.2 kg C $yr^{-1}m^{-2}$ floor area in SFD built between 1965 and 1990 and 6.3 kg C $yr^{-1}m^{-2}$ floor area in more recently developed SFDs (post 1990), reflecting both, larger built volumes of newer dwellings, changes in occupancy (more secondary suites in newer dwellings), changes in heating system efficiency, better insulation and improved air-tightness. In the current implementation of the BEM, spatial differences in energy use due to actual occupant behavior, local building shape and local shading are unaccounted for, although those might be important factors (e.g. Ratti et al., 2005). Fireplaces are not modelled in the BEM either, but are estimated only a minor source (wood burning is estimated ~0.01 kg C m^{-2} yr^{-1}). A map of the spatial distribution of building emissions is shown in Fig. 3a. All results consider local emissions only (i.e. natural gas combustion).

3.1.2. Transportation

In the study area, 2.93 kg C m^{-2} yr^{-1} are estimated to be emitted from the transportation sector. It is clear from the map in Fig. 3b that arterial roads are emission 'hot spots', where, from a relatively small

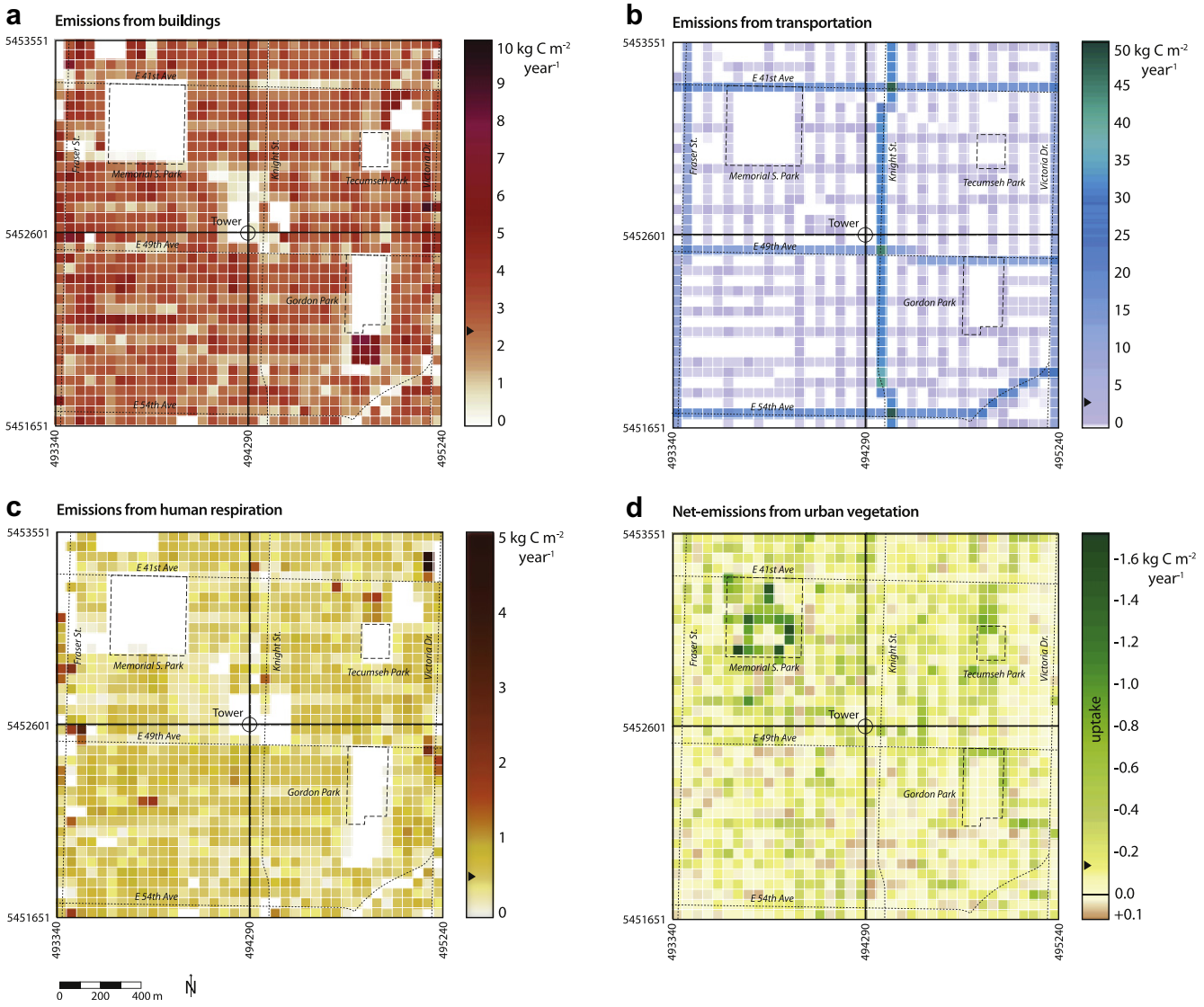

Fig. 3. Raster maps of annual total (local) CO_2 emissions at 50 m grid resolution for (a) buildings, (b) transportation, (c) human respiration and (d) vegetation. Negative numbers for vegetation indicate uptake. Triangles in the legend indicate the spatial mean of the entire neighborhood.

area, significant emissions are released. Out of all transportation emissions, only 11% (0.31 kg C m^{-2} yr^{-1}) are attributable to trips within the study area with the remainder (89%; 2.62 kg C m^{-2} yr^{-1}) to trips passing through the study area. As all emissions (local and through) will be measured by the tower, they are both included in the validation. Emissions from small gardening equipment (lawn mowers, leaf blowers, trimmers etc.) were not accounted in traffic counts. Estimates based on the EPA NONROAD2008 model settings suggest emissions of ~0.03 kg C m^{-2} yr^{-1} from gardening equipment.

3.1.3. Human respiration

CO_2 emission due to human respiration was estimated as 0.49 kg C m^{-2} yr^{-1} and the spatial map of this component, which reflects the night-time population distribution, is shown in Fig. 3c. Uncertainties are in part due to residents that move and work outside the neighborhood and other people that are working in or commuting through the neighborhood – both cases are not accounted for.

3.1.4. Vegetation and soils

The neighborhood-wide emissions due to soil and lawn respiration were calculated as 0.28 g C m^{-2} yr^{-1}. This value includes autotrophic respiration of lawns and tree roots. Autotrophic above ground respiration of trees was and estimated 0.05 kg C m^{-2} yr^{-1}. The sum of soil, lawn, and tree respiration was 0.33 g C m^{-2} yr^{-1} and contributes 5% to all local emissions.

Photosynthesis was found to be −0.21 kg C m^{-2} yr^{-1} for lawns and −0.28 kg C m^{-2} yr^{-1} for trees (negative value implies a carbon uptake), resulting in a direct net exchange in the neighborhood of 0.33 (respiration) − 0.49 (photosynthesis) = −0.16 kg C m^{-2} yr^{-1}. Note that part of the CO_2 taken up (0.07 kg C m^{-2} yr^{-1}) is expected to be removed by export of litter and clippings (assuming typical values), so actual ecosystem sequestration is estimated about −0.09 kg C m^{-2} yr^{-1}. The net effect of respiration and photosynthesis is shown in Fig. 3d where negative values indicate a net uptake.

3.1.5. Integrated emissions

The summed local emission components (buildings, transportation, human metabolism, and the net effects of vegetation/soils, Sections 3.1.1–3.1.4) are shown in Fig. 4a. From the emitted total of 6.22 kg C m^{-2} yr^{-1} in the study area, 40% originate from buildings, 47% from transportation, 8% from human respiration and 5% from respiration of soil and vegetation. Those emissions are partially offset by an annual uptake of 0.49 kg C m^{-2} yr^{-1} through photosynthesis of urban vegetation (lawns and trees). Out of the local *fossil fuel emissions* in the study area, 46% originate from the building sector, whereas 54% are from the transportation sector. The integrated map of emissions (Fig. 4a) is used as the basis for the validation process using direct EC measurements in Section 3.3.

Fig. 4b illustrates the relative contribution from three major emission sectors (buildings in red, transportation in blue, and respiration in green) for each 50 m raster element. Respiration is the sum of human respiration, soil respiration and vegetation respiration but does not include CO_2 uptake by photosynthesis. Buildings are the dominant source (midblock) with the exception of arterial roads (transportation) and parks (respiration).

3.2. Direct flux measurements

Table 2 (first column) summarizes monthly measured CO_2 fluxes in g C m^{-2} day^{-1} for the average of all four wind sectors. The largest emissions were recorded in the winter months (maximum in December with 22.1 g C m^{-2} day^{-1}) when space-heating requirements are expected to be highest and CO_2 uptake from vegetation is minimal. The monthly minimum recorded was 16.0 g C m^{-2} day^{-1} in August during school holidays. The annual average was 18.4 g C m^{-2} day^{-1}, which corresponds to 6.71 kg C m^{-2} yr^{-1}. Those fluxes agree well with summertime values reported in Walsh (2005) who measured F_c at the same location on the same tower in 2002 using a closed-path CO_2 analyzer and a different sonic anemometer. Aggregating her values into the same four sectors (data was initially binned in eight sectors), results in good agreement during summer months. The average reported for the period Apr to Sep 2002 in Walsh (2005) is 14.2 g C m^{-2} day^{-1} while the current study measured 16.8 g C m^{-2} day^{-1} (2008–2009). The difference is partially explained by frequency loss in the >30 m long tube of the closed-path analyzer and the lack of a sensor separation correction in 2002. Annual CO_2 emissions reported from measurements at similar scale in different cities are + 0.36 kg C m^{-2} yr^{-1} in a low-density

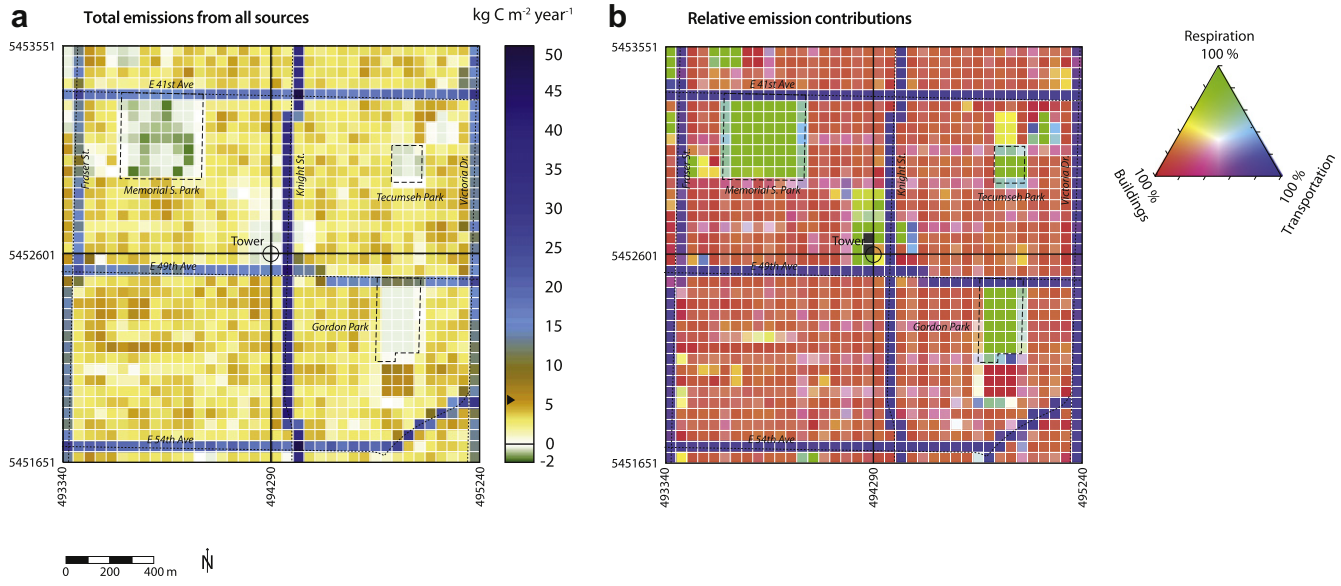

Fig. 4. Raster maps of (a) annual total (local) CO_2 emissions from all sources and (b) RGB composite map of relative contributions of local CO_2 emission sources – buildings (red), transportation (blue) and respiration (green, human and soil respiration combined) to the total emissions from each raster cell.

Table 2
Comparison of measured and modeled CO_2 emissions (source area weighted) on a monthly basis. Percentages in brackets below the annual total refer to the relative contribution of the component to the sum of all modeled emissions. Negative numbers under vegetation are a net uptake.

	Measured ($g\ C\ m^{-2}\ day^{-1}$)	Total modeled ($g\ C\ m^{-2}\ day^{-1}$)	Difference ($g\ C\ m^{-2}\ day^{-1}$)	Modeled buildings ($g\ C\ m^{-2}\ day^{-1}$)	Modeled transportation ($g\ C\ m^{-2}\ day^{-1}$)	Modeled human respiration ($g\ C\ m^{-2}\ day^{-1}$)	Modeled vegetation/soil ($g\ C\ m^{-2}\ day^{-1}$)
Jan	20.9	24.2	3.3	10.3	13.1	1.0	−0.1
Feb	20.0	23.7	3.7	8.9	14.1	1.0	−0.3
Mar	20.2	22.3	2.1	7.4	14.3	1.0	−0.4
Apr	18.2	19.2	1.0	5.2	14.4	1.0	−1.3
May	17.0	17.6	0.6	3.2	14.8	1.0	−1.3
Jun	16.3	17.1	0.8	2.1	15.2	0.9	−1.1
Jul	16.8	17.1	0.3	1.7	15.1	1.0	−0.7
Aug	16.0	17.5	1.5	1.7	15.3	1.0	−0.5
Sep	16.4	17.4	1.0	2.3	14.6	1.0	−0.5
Oct	17.8	20.4	2.6	5.0	14.1	1.0	0.2
Nov	19.0	23.3	4.3	8.4	13.7	1.0	0.2
Dec	22.1	24.4	2.3	10.3	13.1	1.0	0.0
Year ($kg\ C\ m^{-2}\ year^{-1}$)	6.71	7.46	+0.75	+2.02 (27%)	+5.22 (70%)	+0.36 (5%)	−0.17 (−2%)

suburban area in Baltimore (Crawford et al., 2011), +2.31 kg $C\ m^{-2}\ yr^{-1}$ in a mid-density residential neighborhood of Melbourne, Australia (Coutts et al., 2007), + 2.94 kg $C\ m^{-2}\ yr^{-1}$ in a compact residential midrise area in Łódź, Poland (Pawlak et al., 2010), +3.35 kg $C\ m^{-2}\ yr^{-1}$ in a compact residential area of Tokyo (Moriwaki and Kanda, 2004), and +3.94 kg $C\ m^{-2}\ yr^{-1}$ for a densely urbanized wind sector of a flux tower in Essen, Germany (Kordowski and Kuttler, 2010). The current site with 6.71 $kgC\ m^{-2}\ yr^{-1}$ is higher than all those previous studies, reflecting likely the tower's proximity to major arterial roads, and the high occupancy, both which are higher than in most of the other sites reported above. Further, the tower captures significant emissions that are not due to local (residential) activities but originating from trough traffic.

Fig. 5 shows the measured monthly totals of all 24 months 2008–2010 against heating degree days (HDD, air temperature measured at 2 m in the study area). The measured carbon emissions increase roughly by 0.35 g C per m^2 for each unit of HDD. Translated to building volume in the footprint of the tower (derived by LiDAR), this corresponds to 0.32 g C m^{-3} HDD^{-1} or 74 g C $cap^{-1}HDD^{-1}$ (residential population density weighted by the source area is 47 inhabitants ha^{-1}).

When stratifying emission measurements into weekends and weekdays (Fig. 6), emissions were found always to be lower on weekends for all wind sectors and months, with greatest differences observed for the SE sector (on average −9.6 g C m^{-2} day^{-1}, −25% of weekday emissions), intermediate values for NW (−6.8 g C m^{-2} day^{-1}, −30%), and only minor reductions for SW (1.8 g C m^{-2} day^{-1}, −14%) and NW (−1.3 g C m^{-2} day^{-1}, −19%). Note that only months with sufficient statistical data on weekends are shown in Fig. 6 (e.g. only 3 months for NW).

3.3. Comparison of measured and modeled CO_2 fluxes

Tables 3 and 4 compare CO_2 fluxes measured on the tower F_c to modeled emissions M_c. The model results used for the comparison

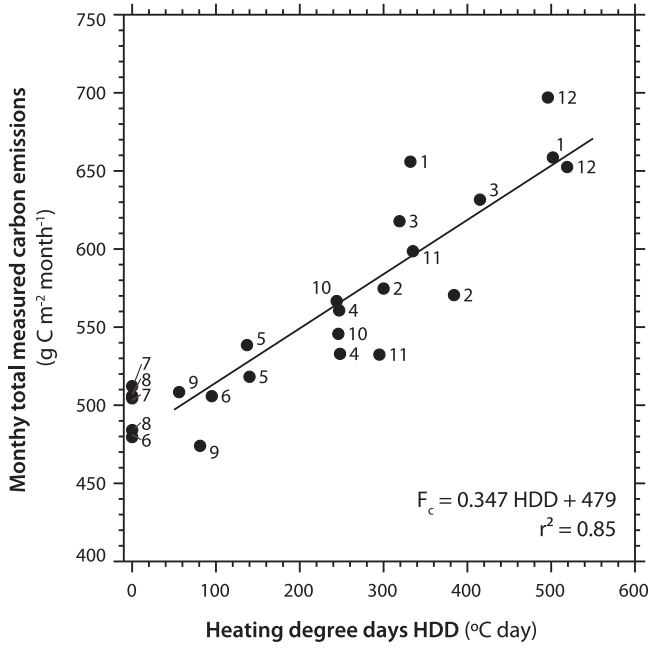

Fig. 5. Monthly total carbon emissions as a function of measured heating degree days (total of the given month) for all 24 months of the study period. The numbering of the markers refers to the month of the year (1 – January to 12 – December).

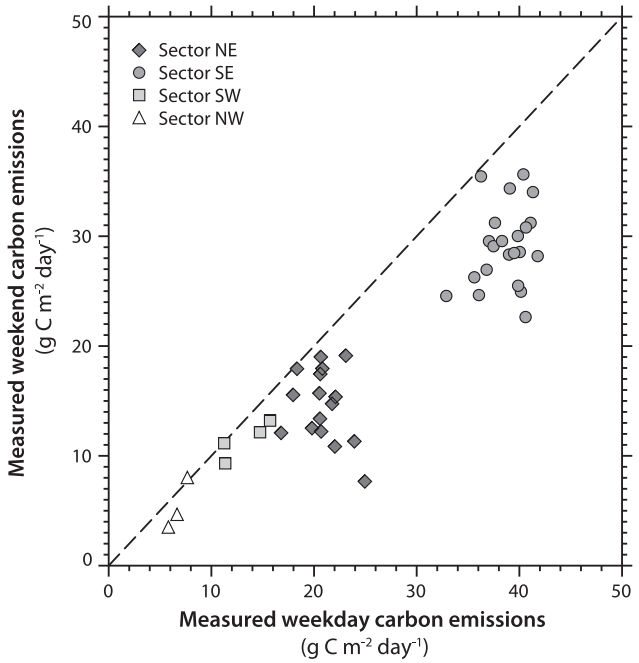

Fig. 6. Measured weekday vs. weekend carbon emissions for all 24 months of the study period. Only months that have complete datasets without gaps are shown.

Table 3
Comparison of modeled and measured carbon emissions for a 400 m radius buffer around the tower. Percentages in brackets refer to the relative contribution of a component to the sum of all modeled emissions.

	All	NE	SE	SW	NW
Measured emissions (kg C m^{-2} $year^{-1}$)	6.71	6.57	13.16	4.31	2.81
Total modeled emissions (kg C m^{-2} $year^{-1}$)	6.46	7.62	10.17	5.81	2.27
Modeled buildings emissions(kg C m^{-2} $year^{-1}$)	2.40 (37%)	2.06 (27%)	2.67 (26%)	3.03 (52%)	1.82 (80%)
Modeled transportation emissions (kg C m^{-2} $year^{-1}$)	3.76 (58%)	5.29 (69%)	7.13 (70%)	2.31 (40%)	0.35 (15%)
Modeled human respiration (kg C m^{-2} $year^{-1}$)	0.47 (7%)	0.45 (6%)	0.51 (5%)	0.61 (11%)	0.29 (13%)
Modeled vegetation/soil net-emissions (kg C m^{-2} $year^{-1}$)	−0.16 (−3%)	−0.18 (−2%)	−0.14 (−1%)	−0.15 (−2%)	−0.19 (−8%)
Difference total modeled − measured (kg C m^{-2} $year^{-1}$)	−0.25	+1.05	−2.99	+1.50	−0.54
Difference (percentage)	−4%	+16%	−23%	+35%	−19%

are aggregated in two different ways. In a simple approach ('*Radius Aggregation*' Section 3.3.1 and Table 3), all grid cells of the 50m raster that fall within a 400 m radius around the tower are averaged with equal weights. Those values are then compared to the tower measurements. A 400 m radius was chosen because this corresponds to the 50% turbulent source area and includes the maximum of $\phi\,(x,y)$ in most cases.

In a more sophisticated aggregation approach ('*Source-area aggregation*', Section 3.3.2, Table 4), model emissions $M_c\,(x,y)$ are weighted by the actual distribution of the turbulent flux footprint $\phi\,(x,y)$.

3.3.1. Radius aggregation

For the average of all emissions within a 400 m radius buffer around the tower, the model results agree well with the measurements, 6.71 kg C m^{-2} yr^{-1} measured vs. 6.46 kg C m^{-2} yr^{-1} modeled (Table 3). The model slightly underestimates measured emissions by 0.25 kg C m^{-2} yr^{-1} (or 4%). With the actual errors associated with the simplification of a 400 m buffer source area, this is a promising result. The model results are split up into different components in Table 3.

Comparing the four wind sectors within the 400 m radius buffer reveals higher discrepancies, in particular for the SE sector, where measurements are higher (13.16 kg C m^{-2} yr^{-1}) than modeled values (10.17 kg C m^{-2} yr^{-1}). This might be an over-proportional contribution of traffic-related emissions from a near-field intersection (49th Ave./Knight St. with traffic lights) where both idling and slowly moving vehicles are injecting more CO_2 into the atmosphere than the average road segment. Different vehicle speed is not accounted for in the transportation model. In turn, in the two sectors that show arterial road segments without intersections, and where a higher average vehicle speed can be expected (NE and SW), the model overestimates emissions (by 16% and 35% respectively). Improving the transportation model and incorporating speed of vehicles in each cell might resolve some of those discrepancies.

3.3.2. Source-area aggregation

The source area aggregation is more meaningful than the 400 m radius buffer method because a significant portion of the measured emissions originate beyond the 400 m boundary, and also the probability density for emissions to originate within the 400 m buffer varies. The source areas represent the diminishing contributions of far-field areas rather than applying an abrupt and unrealistic cut-off at 400 m. The two-year integrated source area of the EC system is shown in a 50 m grid in Fig. 7a and is also overlaid as contours in Fig. 1. Approximately 50% of the measured signal is from within 400 m of the tower, 88% is within the study area. This source area is composed of primarily residential dwellings and also includes the busy intersection of Knight Street and 49th Avenue (87,000 vehicles day^{-1}).

The source-area weighted model grid is shown in Fig. 7b. The map in Fig. 7b is the multiplication of the maps in Figs. 7a and 4a and shows the CO_2 flux contribution ($[M_c]_{in}$). Integrated over the entire map 7b, $[M_c]_{total}$ is 7.46 kg C m^{-2} yr^{-1}(11% higher than the measured 6.71 kg C m^{-2} yr^{-1}). The source area model combined with the emission model suggests that approximately 70% of all fluxes that were measured at the tower (5.22 kg C m^{-2} yr^{-1}) originate from transportation (restricted to a narrow subset of the area around the intersection of Knight and 49th Avenue, see Fig. 5b). Of the remaining fluxes, 27% (2.05 kg C m^{-2} yr^{-1}) originate from buildings, 5% from human respiration and −2% (−0.17 kg C m^{-2} yr^{-1}) is offset by vegetation. Although in the entire 1900 m by 1900 m study area, emissions from buildings and transportation are of approximately equal strength (40% and 47% of all emission, see Section 3.1), the specific location of the tower close to an intersection makes the signal from transportation in the tower signal more relevant. Interestingly, the sector where transportation emissions are small (NW) shows an exceptional agreement between tower and model (2.81 kg C m^{-2} yr^{-1} measured vs. 2.87 kg C m^{-2} yr^{-1} modeled), again suggesting that the transportation sub-model might be less detailed in the geographic

Table 4
Comparison of modeled and measured CO_2 emissions weighted by the long-term turbulent source area of the tower. Percentages in brackets refer to the relative contribution of a component to the sum of all modeled emissions.

	All	NE	SE	SW	NW
Measured emissions (kg C m^{-2} $year^{-1}$)	6.71	6.57	13.16	4.31	2.81
Total modeled emissions (kg C m^{-2} $year^{-1}$)	7.46	9.40	11.41	6.18	2.87
Modeled buildings emissions (kg C m^{-2} $year^{-1}$)	2.05 (27%)	1.93 (21%)	2.36 (21%)	2.36 (38%)	1.55 (54%)
Modeled transportation emissions (kg C m^{-2} $year^{-1}$)	5.22 (70%)	7.32 (78%)	8.81 (77%)	3.53 (57%)	1.22 (42%)
Modeled human respiration (kg C m^{-2} $year^{-1}$)	0.36 (5%)	0.32 (3%)	0.40 (3%)	0.45 (7%)	0.27 (9%)
Modeled vegetation/soil net-emissions (kg C m^{-2} $year^{-1}$)	−0.17 (−2%)	−0.17 (−2%)	−0.16 (−1%)	−0.16 (−3%)	−0.17 (−6%)
Difference total modeled − measured (kg C m^{-2} $year^{-1}$)	+0.75	+2.83	−1.75	+1.87	+0.06
Difference (percentage)	+11%	+43%	−13%	+43%	+2%

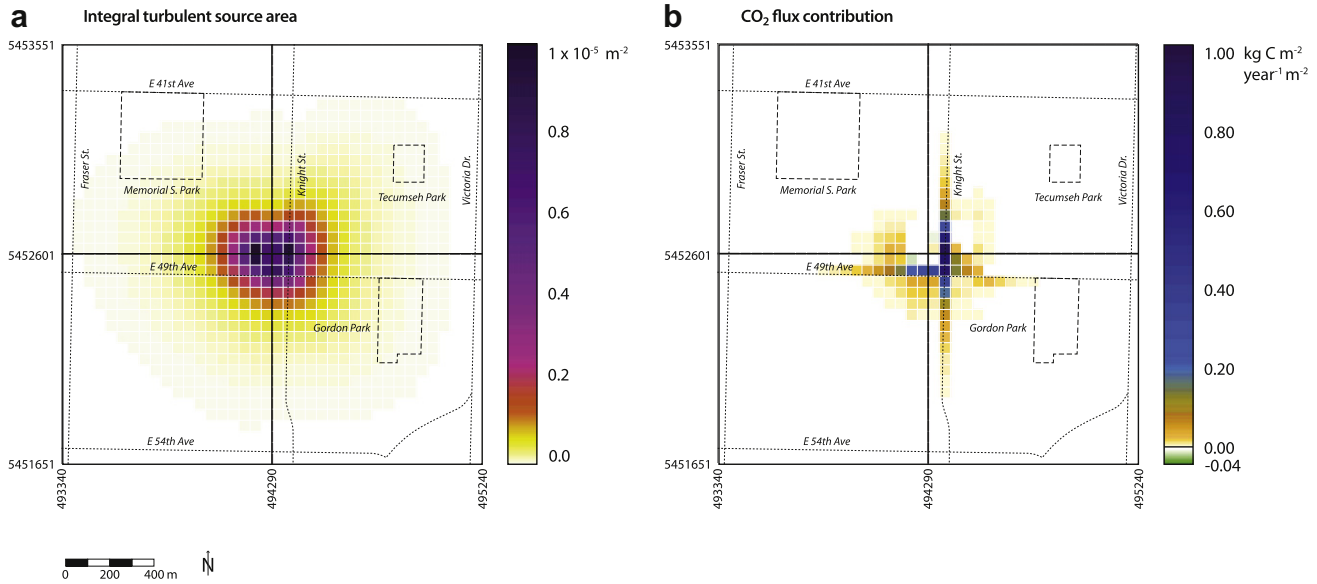

Fig. 7. Raster maps of (a) integral turbulent source area for the period May 1, 2008 to April 30, 2010 (b) source-area weighted CO_2 fluxes (flux-contributions, product of maps Figs. 4a and 3a).

distribution of emissions, i.e. vehicles are incorrectly expected to emit per arterial road segment instead of moving faster along straight arterial road sections (lower emissions per m^2) and idling at intersections (higher emissions).

3.3.3. Comparison of seasonal variations

Table 2 and Fig. 8 compare modeled against measured fluxes for each month separately. Each month is the average of measurements in the given month in both years of the study. For all monthly values the root mean square error (RMSE) is 2.11 g C m^{-2} day^{-1} (13% of the yearly average fluxes).

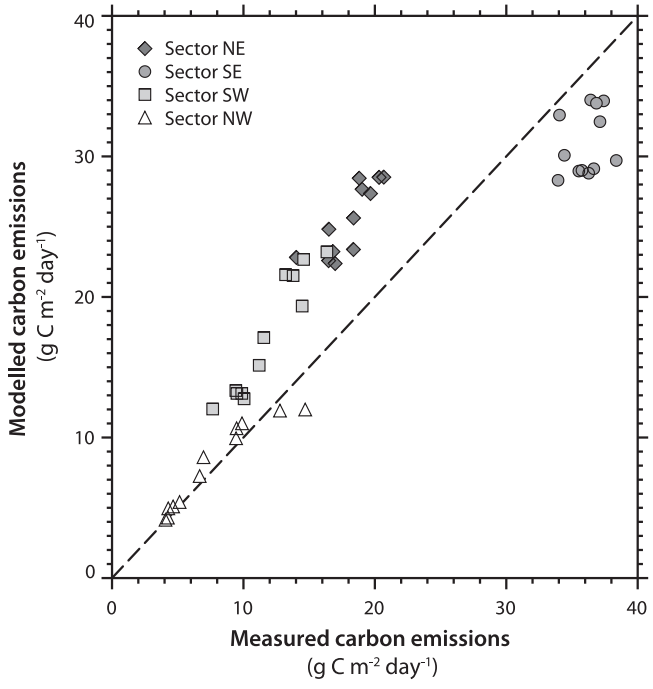

Fig. 8. Modeled vs. measured carbon emissions separately compared for all wind sectors (see legend). Each marker corresponds to one month averaged over two years.

It is evident from Table 2 that the summer values are in closer agreements (Apr–Sep, +5% overestimation by the model), while winter months agree less with the measured values (Oct–Mar, +15% overestimation).

This comparison suggests that the building sub-component, the vegetation effects and/or the annual traffic profile have also minor deficiencies. The building energy model results show an increase in heating-related emissions per building volume of 0.56 g C m^{-3} HDD^{-1}, while the statistical relation derived from the measurements in Fig. 5 shows 0.32 g C m^{-3} HDD^{-1} (Section 3.2). Attributing the relation of 0.32 g C m^{-3} HDD^{-1} in Fig. 5 to the building sector only is not correct, as with increasing HDD (decreasing temperature, decreasing PAR) vegetation will also store less carbon (and eventually turn into a source), but also transportation emissions are expected to decrease by about 10% in winter relative to summer.

The building energy models use 30-year average temperatures measured at Vancouver Airport, which adds two additional potential errors to the model: (a) the study period experienced different weather than the 30-year average, and (b) effects of the urban heat island (UHI) causing elevated average temperatures in the urban area compared to the airport. Although the average temperature in the two-year period was only 0.2 K warmer than the 30-year climatology, winter months (Nov–Feb) were 0.4 K warmer than average at the airport which results in 42 HDD less in the study period than in the 30 year average record. This translates to roughly a model overestimation of 0.04 kg C m^{-2} yr^{-1} (modeled building emissions overestimated by 1.7%) in the entire study area. The average temperature difference between the neighborhood

Table 5
Comparison of measured CO_2 emission reduction on weekends to the modeled transportation sector emissions for a 400-m-radius buffer around the tower. Not enough measurements on weekends with wind from the NW were available to estimate the reduction in the NW sector.

	All	NE	SE	SW
Modeled flux density from transportation (g C m^{-2} day^{-1})	13.15	14.1	19.1	6.2
Measured difference between weekday-weekend (g C m^{-2} day^{-1})	5.71	7.31	9.79	5.59
Measured weekend reduction to total modeled transportation flux (%)	42%	38%	48%	40%

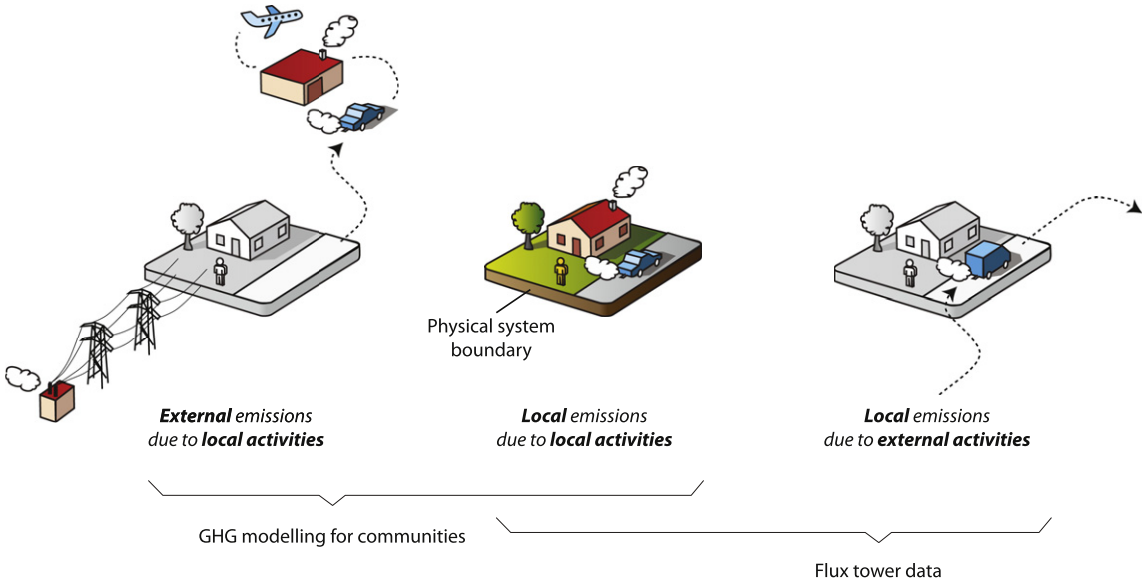

Fig. 9. The concept of local and external emissions for a given urban ecosystem. Note that the flux tower measured a different flux than is needed for informing planning decisions at the neighborhood scale.

and the airport (UHI) was 0.47 K in the two-year period (138 HDD less in the city that at the airport), which translates into an additional model overestimation of 0.12 kg C m^{-2} $year^{-1}$ (5% of building emissions) in the study area. In other words, the urban heat island effect reduces emissions in the study area by 1.2 t C ha^{-1} $year^{-1}$ or 18.6 kg C cap^{-1} yr^{-1}. Note that space cooling is insignificant in this neighborhood. Further, the above relation allows us to estimate errors associated with missing data of the EC system. 30% of the data were missing during rainy or snowy conditions, which are times when air temperature is lower (snow, rain) - on the annual average air temperature during periods when EC data is missing is 0.97K lower compared to periods when EC data is available. This means that actual monthly temperatures are $0.3 \times 0.97 = 0.29$ K lower than during the period when valid EC data exists. This corresponds to a 'missing' additional expected flux of 0.04 kg C m^{-2} yr^{-1} (0.6% of the measured annual total).

When comparing different wind sectors on a monthly basis (Fig. 8, Table 4), the same pattern emerges as reported in Section 3.3.1 - consistently sectors NE and SW are overestimating measured emissions, while emissions in the SE sector (intersection) are underestimated. Best model performance is found in the NW sector with an RMSE of the monthly modeled vs. measured values of 1.11 g C m^{-2} day^{-1} (14% of the sector average).

3.3.4. Weekend-weekday differences

Table 5 compares the observed emission reduction weekend minus weekday in three of four sectors to modeled transportation emissions. The relative measured emission reduction on weekends ΔF_c is expressed as a fraction of the modeled CO_2 emissions from the transportation sector $M_{c(transport)}$. On average, the estimated reduction is 42%. This suggests that weekend traffic, due to the lower volume and composition of the fleet, emits 42% less CO_2 than weekday traffic in the study area.

4. Conclusions and outlook

4.1. Conclusions of results obtained

This study validated a neighborhood-scale CO_2 emission model with directly measured CO_2 fluxes using the eddy-covariance approach. Building on a case study for which direct flux measurements have been compiled and aggregated, the chosen study demonstrates that methods of integrating diverse emission and uptake processes (combustion, respiration, photosynthesis), on a range of scales converge surprisingly well with directly measured CO_2 fluxes by the EC method on an annual and monthly scale. Hence, long-term CO_2 flux measurements on urban flux towers, in combination with turbulent source area models are demonstrated to be a method of validation of fine-scale emission inventories/models at the neighborhood scale. Given the errors associated with the uncertainty of the EC method, the uncertainty of the source area model, and the uncertainties of the modeling assumptions, the close agreement between tower measurements and model results in this study is a successful and promising outcome. It has been further demonstrated that the temporal and spatial variation can be used to identify model deficiencies and guide further model development. Deficiencies identified include (i) the lack of spatially resolved vehicle speed (intersection, idling effects), and (ii) building energy heating demand overestimation (climate input data, assumptions on building-typology). Future research at this site will use higher temporal resolution (diurnal course) and spatial (source area) variation to refine the information extracted from the tower.

4.2. Restrictions of the approach

From a conceptual view, it is challenging to define proper system boundaries in an urban ecosystem and flux measurements cannot be used directly to inform planning decisions (but can be used to validate and develop models). If assessing the environmental sustainability of a given urban system, we should consider all processes that are part of the urban metabolism, including effects that take place beyond the neighborhood's limits. This conceptual discrepancy between tower measurements and the neighborhood carbon 'footprint' is summarized in Fig. 9. "External emissions due to local activities" refers to the release of CO_2 *outside* the neighborhood (system boundaries) due to combustion or respiration associated with activities within the neighborhood (e.g. electricity generation, travel outside of the neighborhood). "Local emissions due to local activities" refers to the release (or uptake) of CO_2 *within* the neighborhood (system boundaries)

due to combustion, respiration or photosynthesis. "Local emissions due to external activities" - refers to the release of CO_2 *within* the neighborhood (system boundaries) due to combustion and respiration from objects or humans travelling through the neighborhood, but not associated with activities in the neighborhood (e.g. through-traffic). Note the difference between what the tower is measuring (local emissions only) and what are deliverables for GHG modeling (emissions due to local activities). As municipal, regional and national governments strategize to reduce GHG emission, these issues associated with defining system boundaries become important across a range of scales.

Acknowledgements

Principal funding for developing the emission modeling has been provided by CanmetENERGY, Natural Resources Canada, Ottawa (J. Webster, project manager). The Canadian Foundation for Climate and Atmospheric Sciences (CFCAS) funded the acquisition and processing of the LiDAR data as well as the two-year measurements on the flux tower as part of the CFCAS network "Environmental Prediction in Canadian Cities (EPiCC)". Selected research infrastructure on the tower was supported by NSERC RTI (Christen) and CFI/BCKDF (Christen). We acknowledge the support of BC Hydro, the City of Vancouver and Environment Canada for providing additional data. We further acknowledge the significant technical and administrative support of staff at the University of British Columbia including J. Bau, E. Heyman, R. Ketler, S. Lapsky, Z. Nesic, J. Ranada, C. Siemens.

References

Akbari, H., Pomerantz, A., Taha, H., 2001. Cool surfaces and shade trees to reduce energy use and improve air quality in urban areas. Solar Energy 70, 295–310.

Baker, N., Steemers, K., 2000. Energy and Environment in Architecture: A Technical Design. E&FN Spon., New York, p. 240.

Baldocchi, D.D., 2003. Assessing the eddy covariance technique for evaluating carbon dioxide exchange rates of ecosystems: past, present and future. Global Change Biology 9, 479–492.

Chen, B., Black, T.A., Coops, N.C., Hilker, T., Trofymow, J.A., Morgenstern, K., 2009. Assessing tower flux footprint climatology and scaling between remotely sensed and eddy covariance measurements. Boundary-Layer Meteorology 130, 137–167.

Christen, A., Coops, N., Kellett, R., Crawford, B., Olchovski, I., Tooke, R., van der Laan, M., 2010. A LiDAR-Based Urban Metabolism Approach to Neighbourhood Scale Energy and Carbon Emissions Modeling. Technical Report prepared for Natural Resources Canada. University of British Columbia.

Cleugh, H.A., Oke, T.R., 1986. Suburban–Rural Energy-Balance Comparisons in Summer for Vancouver, BC. Boundary-Layer Meteorology 36, 351–369.

Crawford, B., Christen, A., Grimmond, C.S.B., 2011. Five years of carbon dioxide fluxes measurements in a highly vegetated suburban area. Atmospheric Environment 45, 896–905.

Crawford, B., Christen, A., Ketler, R., 2010. EPiCC Technical Report 1: Processing and Quality Control Procedures of Turbulent Flux Measurements During the Vancouver EPiCC Experiment, EPiCC Technical Report No. 1, p. 15. Retrieved on July 15, 2011 from. http://www.geog.ubc.ca/~epicc/reports/Vancouver-EPiCC-Tech-Report-1.pdf.

Coutts, A.M., Beringer, J., Tapper, N.J., 2007. Characteristics Influencing The Variability of Urban CO_2 fluxes in Melbourne, Australia. Atmospheric Environment 41, 51–62.

Famulari, D., Nemitz, E., Di Marco, C., Phillips, G.J., Thomas, R., House, E., Fowler, D., 2010. Eddy-covariance measurements of nitrous oxide fluxes above a city. Agricultural and Forest Meteorology 150, 786–793.

Goodwin, N.R., Coops, N.C., Tooke, R.T., Christen, A., Voogt, J.A., 2009. Characterising urban surface cover and structure with airborne LiDAR technology. Canadian Journal of Remote Sensing 35, 297–309.

Grazi, F., van den Bergh, J.C.J.M., 2008. Spatial organization, transport, and climate change: comparing instruments of spatial planning and policy. Ecological Economics 67, 630–639.

Grimmond, C.S.B., King, T.S., Cropley, F.D., Nowak, D.J., Souch, C., 2002. Local-scale fluxes of carbon dioxide in urban environments: methodological challenges and results from Chicago. Environmental Pollution 116, S243–S254.

Haltrecht, D., Fraser, K., 1997. Validation of HOT2000 using HERSBESTEST. Proceedings Building Simulation 97, Fifth International IBPSA Conference. Prague, Czech Republic. International Building Performance Simulation Association, September 8–10.

Kalanda, B.D., Oke, T.R., Spittlehouse, D.L., 1980. Suburban energy-balance estimates for Vancouver, BC, using the Bowen ratio-energy balance approach. Journal of Applied Meteorology 19, 791–802.

Kennedy, C., Steinberger, J., Gasson, B., Hansen, Y., Hillman, T., Havránek, M., Pataki, D., 2009. Greenhouse gas emissions from global cities. Environmental Science & Technology 43, 7297–7302.

Kordowski, K., Kuttler, W., 2010. Carbon dioxide fluxes over an urban park area. Atmospheric Environment 44, 2722–2730.

Kormann, R., Meixner, F.X., 2001. An analytical footprint model for non-neutral stratification. Boundary-Layer Meteorology 99, 207–224.

Liss, K., Crawford, B., Jassal, R., Siemens, C., Christen, A., 2009. Soil Respiration In Suburban Lawns And Its Response To Varying Management And Irrigation Regimes. Proc. of the AMS Eighth Conference on the Urban Environment, Phoenix, AZ, January 11–15, 2009.

Liss, K., Tooke, R., Coops, N., Christen, A., 2010. Vegetation Characteristics at the Vancouver EPiCC Experimental Sites, EPiCC Technical Report No. 3, p. 38. Retrieved on June 20, 2010 from. http://www.geog.ubc.ca/~epicc/reports/Vancouver-EPiCC-Tech-Report-3.pdf.

McPherson, E.G., 1994. Cooling urban heat islands with sustainable landscapes. In: Platt, R., Rowntree, R., Muick, P. (Eds.), The Ecological City: Preserving And Restoring Urban Biodiversity. University of Massachusetts Press, Amherst, pp. 151–171.

Moore, C.J., 1986. Frequency response corrections for eddy correlation systems. Boundary-Layer Meteorology 37, 17–35.

Moriwaki, R., Kanda, M., 2004. Seasonal and diurnal fluxes of radiation, heat, water vapor, and carbon dioxide over a suburban area. Journal of Applied Meteorology 43, 1700–1710.

Newman, P., Kenworthy, J., 1989. Cities and Automobile Dependence: An International Sourcebook. Gower, Aldershot, UK, p. 388.

Natural Resources Canada, 2009. Fuel Consumption Guide 2009/Guide de consummation de carburant 2009 Compiled by: Office of Energy Efficiency. Cat. No. M141–5/2009 (Print).

Natural Resources Canada, 2010. Office of Energy Efficiency Screening Tool. http://screen.nrcan.gc.ca/. (accessed 20.06.10).

Nowak, D.J., 1996. Estimating Leaf Area and Leaf Biomass of Open-Grown Deciduous Trees. Forest Science 42, 504–507.

Ögren, E., Evans, J.R., 1993. Photosynthetic light-response curves, 1. The influence of CO_2 partial pressure and leaf inversion. Planta 189, 182–190.

Parshall, L., Gurney, K., Hammer, S.A., Mendoza, D., Zhou, Y.Y., Geethakumar, S., 2010. 'Modeling energy consumption and CO_2 emissions at the urban scale: methodological challenges and insights from the United States. Energy Policy 38, 4765–4782.

Pawlak, W., Fortuniak, K., Siedlecki, M., 2010. Carbon dioxide flux in the centre of Łódź, Poland - analysis of a 2-year eddy covariance measurement data set. International Journal of Climatology 31, 232–242.

Province of British Columbia, 2008. Greenhouse Gas Emissions Assessment Guide for British Columbia Local Governments Version 1. Retrieved on June 20, 2010 from. http://www.localmotion.gov.bc.ca/docs/ghg_assessment_guidebook_feb_2008.pdf.

Ratti, C., Baker, N., Steemers, K., 2005. Energy consumption and urban texture. Energy and Buildings 37, 762–776.

Raupach, M.R., Rayner, P.J., Paget, M., 2009. Regional variations in spatial structure of nightlights, population density and fossil-fuel CO_2 emissions. Energy Policy 38, 4756–4764.

Roth, M., Oke, T.R., Steyn, D.G., 1989. Velocity and temperature spectra and cospectra in an unstable suburban atmosphere. Boundary-Layer Meteorology 47, 309–320.

Satterthwaite, D., 2008. Cities' contribution to global warming: notes on the allocation of greenhouse gas emissions. Environment and Urbanization 20, 539–549.

Salat, S., 2007. Energy and Bioclimatic efficiency of urban Morphologies: towards a Comparative analysis of Asian and European cities. Proceedings of the International Conference on Sustainable Building Asia, Fraunhofer IRB, 161–166.

Simpson, J.R., 2002. Improved estimates of tree-shade effects on residential energy use. Energy and Buildings 34, 1067–1076.

Soegaard, H., Moller-Jensen, L., 2003. Towards a spatial CO_2 budget of a metropolitan region based on textural image classification and flux measurements. Remote Sensing of Environment 87, 283–294.

Statistics Canada, March 13, 2007. Census 2006-Population and Dwelling Counts. Release No. 1.

Tooke, R., Coops, N.C., Goodwin, N.R., Voogt, J.A., 2009. The influence of vegetation characteristics on spectral mixture analysis in an urban environment. Remote Sensing of Environment 113, 398–407.

Velasco, E., Roth, M., 2010. Cities as net sources of CO_2: review of atmospheric CO_2 exchange in urban environments measured by eddy covariance technique. Geography Compass 4, 1238–1259.

VandeWeghe, J.R.A., Kennedy, C., 2008. Spatial Analysis Of Residential Greenhouse Gas Emissions In The Toronto Census Metropolitan Area. Journal of Industrial Ecology 11, 133–144.

Walsh, C. J., 2005. Fluxes of radiation, energy, and carbon dioxide over a suburban area of Vancouver, BC. M.Sc. Thesis, Department of Geography, University of British Columbia.

Webb, E.K., Pearman, G.I., Leuning, R., 1980. Correction of flux measurements for density effects due to heat and water vapour transfer. Quarterly Journal of the Royal Meteorological Society 106, 85–100.